

Caging of Short-Range Interactions in All Bands Flat Lattices: Part I

Carlo Danieli,^{1,2} Alexei Andreanov,^{2,3} Thudiyangal Mithun,^{4,2} and Sergej Flach^{2,3}

¹*Max Planck Institute for the Physics of Complex Systems, Dresden D-01187, Germany*

²*Center for Theoretical Physics of Complex Systems, Institute for Basic Science(IBS), Daejeon 34126, Korea*

³*Basic Science Program(IBS School), Korea University of Science and Technology(UST), Daejeon 34113, Korea*

⁴*Department of Mathematics and Statistics, University of Massachusetts, Amherst MA 01003-4515, USA*

(Dated: June 15, 2022)

We study the transport impact of classical and quantum short-range interactions on one-dimensional All-Bands-Flat (ABF) lattices. The single particle band structure of ABF lattices contains flatbands only, and results in caging of non-interacting particles by compact localized eigenstates. Proper unitary transformations lead to a complete detangling of compact localized states. The application of these very unitary transformations to short range Hubbard-type interactions reveals that both quantum and classical (i.e. nonlinear) interactions generally *break* single particle caging and produce transporting states. Here we derive fine-tuning conditions of the single particle Hamiltonian such that both classical and quantum interactions *preserve* caging features. Fine tuning and nonlinear interactions yield exact caging and absence of transport. Quantum interactions result in a mixture of transporting states and macroscopically degenerated compact states, whose eigenenergies are tunable via the interaction strength.

I. INTRODUCTION

Understanding the impact of interactions on single particle localized states has been one of the most intriguing quests of the past decades in condensed matter physics, which produced some of the most productive research streams to date. Notably, classical and quantum approaches may yield seemingly distinct outcomes while starting from the same single particle localization. One notable example concerns the impact of interactions on Anderson localization – i.e. the exponential localization of all single particle states due to uncorrelated disorder [1]. Weakly interacting quantum particles show a finite temperature transition to a many-body localized phase [2–4]. Classical interactions instead predict finite heat and particle conductivity at arbitrarily small temperatures, and related indefinite subdiffusive wave-packet spreading [5, 6].

Anderson localization relies on the presence of disorder. On lattices single particle localization (caging) can be also obtained in the absence of disorder, i.e. for translationally invariant lattice settings. We study the distinct features that emerge from considering classical and quantum interactions in presence of single particle caging in translationally invariant lattices. Caging arises from the collapse of the entire single particle spectrum into a set of Bloch bands with no dispersion – hence flat – due to destructive interference. This collapse of the spectrum defies transport and confines (cages) noninteracting particles within a strictly compact and finite volume of the lattice. These single particle networks are coined All Bands Flat (ABF) networks. They belong to the class of flatband lattices, which have been profoundly studied in recent years due to the interest in spatially compact states related to these flatbands [7, 8]. Recent advances range from systematic generator schemes [9–13] to localization phenomena due to onsite perturbations [14–17], non-hermitian potentials [18, 19], and nonlinear interac-

tions [20–23] among others, and they have been experimentally realized in several setups, e.g. [24–29]. One way to obtain an ABF network is to fine-tune a magnetic field on the diamond (rhombic) chain. Such a set-up – experimentally realized in Ref. 30 using photonic lattices – has been used to study both classical and quantum interactions. While nonlinear interactions preserve caging [31, 32], quantum Hubbard interactions induce transporting bound states of two particles [33].

In this work, we study both classical and quantum interactions on generic ABF networks, choosing $\nu = 2$ bands networks as testbeds. We show that in the absence of interactions, proper unitary transformations lead to a complete detangling of the network into decoupled sites. Secondly, we employ these unitary transformations to show that both nonlinear and quantum interactions in general break the linear single particle caging and result in transport and delocalization. We then obtain fine-tuning conditions such that both nonlinear and quantum interactions preserve caging features. The intricate caging features arising from quantum interactions will be unfolded in a subsequent work [34].

II. GENERATING SINGLE PARTICLE CAGING

Let us consider the time-dependent equations of a one-dimensional generalized tight-binding problem

$$i\dot{\psi}_n = -H_0\psi_n - H_1\psi_{n+1} - H_1^\dagger\psi_{n-1}. \quad (1)$$

For any $n \in \mathbb{Z}$, each component of the complex vector $\psi_n = (\psi_{n,1}, \dots, \psi_{n,\nu})^T$ represents a site of the periodic lattice, and therefore ψ_n represents its *unit cell*. The profile of the network is defined by the square matrices H_0, H_1 . The transformation $\psi_n = x_n e^{-iEt}$ yields the eigenvalue problem associated to Eq. (1), and then the Bloch solution $x_n = e^{ikn} y_k$ defined for the wave-vector \mathbf{k} gives rise to the band structure $\{E_j(\mathbf{k})\}_{j=1}^\nu$ of

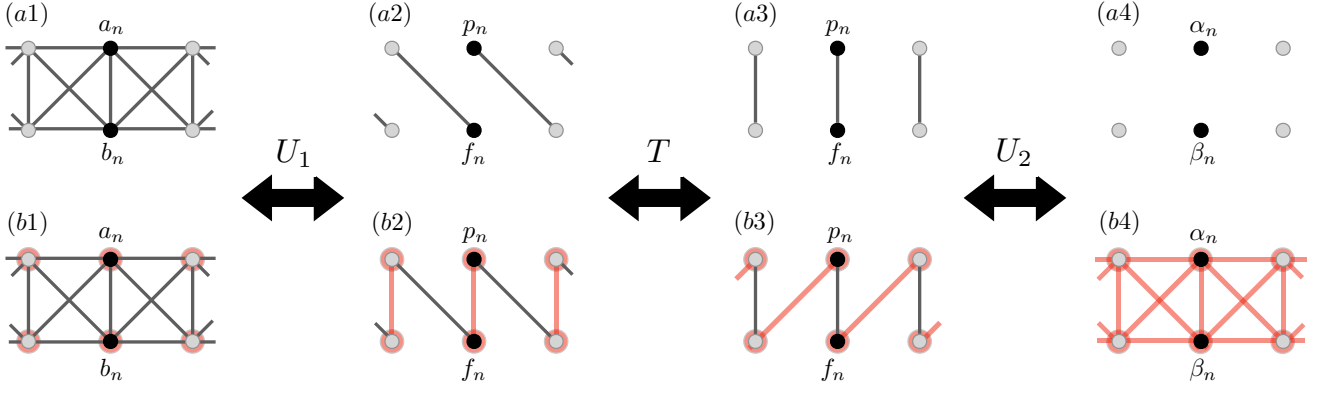


FIG. 1. (Color online) Schematic representation of the unit cell redefinition for a $\nu = 2$ ABF lattice. In each panel, the black dots label the chosen unit cell. The solid gray lines represent the linear hopping terms; the red shaded lines represent the interaction terms. (a1)-(a4) Noninteracting regime. (b1)-(b4) Interacting regime.

Eq. (1). In this work we focus on ABF networks where all bands E_j are independent on \mathbf{k} - hence all bands are flat. The collapse of the single-particle spectrum into several flatbands and the absence of dispersive states is coined caging. Any compact initial condition remains confined within a finite (compact) sub-volume of the network $\psi_n(t) \neq 0$ for $1 \leq n \leq M$ and $\psi_n(t) = 0$ otherwise, for all $t \in \mathbb{R}$.

With only compact localized eigenstates, Eq. (1) can be always recast into fully decoupled lattice equations

$$i\dot{\phi}_n = H_R \phi_n \quad H_R = \text{diag}(E_1, E_2, \dots, E_\nu) \quad (2)$$

via a suitable redefinition of the unit-cell $\psi_n \mapsto \phi_n$ and a sequence of nested unitary transformations (see Appendix A 1 for the proof and further details). This result holds for any number of bands in a one-dimensional ABF lattice with short-range hopping.

Reversing this procedure $\psi_n \mapsto \phi_n$ yields a generator for any-dimensional networks with all bands flat. This is visualized in Fig. 1(a1)-(a4) for $\nu = 2$ networks, with the canonical coordinates $\psi_n = (a_n, b_n)$ and the detangled coordinates $\phi_n = (\alpha_n, \beta_n)$. The detangling procedure $\psi_n \mapsto \phi_n$ unfolds in three steps

$$\begin{pmatrix} a_n \\ b_n \end{pmatrix} \xrightarrow{U_1} \begin{pmatrix} p_n \\ f_n \end{pmatrix} \xrightarrow{T} \begin{pmatrix} p_n \\ f_n \end{pmatrix} \xrightarrow{U_2} \begin{pmatrix} \alpha_n \\ \beta_n \end{pmatrix} \quad (3)$$

with the alternation of two unitary transformations U_1 and U_2 and one relabeling of the lattice sites T :

$$U_i = e^{i\theta_i} \begin{pmatrix} z_i & w_i \\ -w_i^* & z_i^* \end{pmatrix} \quad T: \begin{cases} p_n \mapsto p_n \\ f_n \mapsto f_{n-1} \end{cases} \quad (4)$$

The complex numbers z_i, w_i are constrained with $|z_i|^2 + |w_i|^2 = 1$. Without loss of generality the two flatband energies can be locked at $E = \pm 1$. We then parametrize the matrices H_0, H_1 for $\nu = 2$ ABF networks in Eq. (1)

as

$$H_0 = \Gamma_0 \begin{pmatrix} |z_1|^2 - |w_1|^2 & -2z_1 w_1 \\ -2z_1^* w_1^* & |w_1|^2 - |z_1|^2 \end{pmatrix} \quad (5)$$

$$H_1 = \Gamma_1 \begin{pmatrix} z_1 w_1^* & z_1^2 \\ -(w_1^*)^2 & -z_1 w_1^* \end{pmatrix} \quad (6)$$

with $\Gamma_0 = |w_2|^2 - |z_2|^2$ and $\Gamma_1 = 2z_2 w_2$ (see Appendix A 2 for details).

We will focus on the parametrized class of $\nu = 2$ ABF networks as a testbed to study caging phenomena induced by classical and quantum interactions respectively. Extensions to larger number of bands, and higher dimensionalities appear straightforward, though increasingly cumbersome.

III. NONLINEAR INTERACTION: SUB-DIFFUSION AND FINE-TUNED CAGING

We start with classical cubic nonlinear interactions which result from mean-field approximations to many-body interacting systems. Equation (1) with $\psi_n = (a_n, b_n)$ turns to

$$i\dot{\psi}_n = -H_0 \psi_n - H_1 \psi_{n+1} - H_1^\dagger \psi_{n-1} + U \mathcal{F}(\psi_n) \psi_n, \quad (7)$$

with $\mathcal{F}(\psi_n) = \begin{pmatrix} |a_n|^2 & 0 \\ 0 & |b_n|^2 \end{pmatrix}$.

These Gross-Pitaevski-type lattice equations can be written in a vector form $i\dot{\psi}_n = \nabla_{\psi_n^*} \mathcal{H}_G$. They are generated by the Hamiltonian $\hat{\mathcal{H}}_G = \hat{\mathcal{H}}_0^G + \hat{\mathcal{H}}_1^G$:

$$\hat{\mathcal{H}}_0^G = - \sum_{n \in \mathbb{Z}} \left[\frac{1}{2} (\psi_n^{*T} H_0 \psi_n) + (\psi_n^{*T} H_1 \psi_{n+1}) + \text{h.c.} \right], \quad (8)$$

$$\hat{\mathcal{H}}_1^G = \frac{U}{2} \sum_{n \in \mathbb{Z}} [|a_n|^4 + |b_n|^4]. \quad (9)$$

By applying the coordinate redefinition $\psi_n \mapsto \phi_n$ to Eq. (7), the local nonlinear terms in the original coordinates ψ_n turn nonlocal in the new coordinates - as sketched in Fig. 1(b1)-(b4). Eq. (7) in the new coordinates ϕ_n reads

$$i\dot{\phi}_n = H_R \phi_n + g\mathcal{P}(\phi_n, \phi_{n+1}, \phi_{n-1}), \quad (10)$$

where H_R is the diagonal matrix in Eq. (2) and \mathcal{P} a homogeneous polynomial of order three in $\{\phi_n, \phi_{n\pm 1}\}$. The polynomial \mathcal{P} defines a nonlinear network between ϕ_n and the neighboring unit-cells $\phi_{n\pm 1}$ - red shaded lines in Figs. 1(b4) - and it generally contains terms that depend solely on $\phi_{n\pm 1}$ (dubbed *fully nonlocal terms*). These terms induce nonlinear transport along the system, and consequently they lift linear (single particle) caging. In the following we present the necessary and sufficient conditions for the vanishing of the fully nonlocal terms which yields suppression of nonlinear transport and establishes nonlinear caging.

A. Necessary and sufficient conditions for nonlinear caging

The phenomenon of nonlinear caging - similarly to linear caging - requires that any spatially compact excitation remains confined for all times. We seek for conditions under which compact excitations such as

$$\begin{cases} \phi_n(t=t_0) \neq 0 & |n| \leq M \\ \phi_n(t=t_0) = 0 & |n| > M \end{cases} \quad (11)$$

stay confined within a finite sub-volume for all times $t > t_0$. Nonlinear caging fails in the presence of fully nonlocal terms in the R.H.S. of Eq. (10), i.e. terms that depend exclusively on neighboring cell wave functions $\phi_{n\pm 1}$. Such terms vanish from Eq. (10) if the condition

$$|w_1|^2 = |z_1|^2 \quad (12)$$

in Eqs. (5, 6) holds (Appendix B1). Then the Hamiltonian $\hat{\mathcal{H}}_1^G$ in Eq. (9) recast via the transformations U_1 and T in Eqs. (3,4) is represented by the density elements (p_n, f_n) (see Appendix B2)

$$\begin{aligned} \mathcal{H}_1^G = U \sum_n \{ & |z_1|^4 [|p_n|^4 + |f_n|^4 + 4|p_n|^2 |f_{n+1}|^2] \\ & + z_1^{*2} w_1^2 p_n^{*2} f_{n+1}^2 + z_1 w_1^{*2} p_n^2 f_{n+1}^{*2} \}. \end{aligned} \quad (13)$$

Consequently, the condition Eq. (12) in Eqs. (5,6) highlights a fine-tuned subclass of nonlinear lattices where the evolution of any initial state which carries a subset of sites with strictly zero densities will keep the densities at these sites strictly zero. The number of sites with vanishing amplitudes is therefore preserved during the dynamics. An initially compact state which has zero amplitudes (densities) outside a finite volume stays strictly compact under classical nonlinear evolution. Likewise,

disconnected compact states stay disconnected. This is the essence of nonlinear caging. We now test this prediction numerically by studying two cases of the set of networks parametrized via Eqs. (5,6) - one which satisfies Eq. (12) and one which does not.

B. Two Examples

We generate two examples by setting $z_i = \cos \varphi_i$, $w_i = \sin \varphi_i$ in Eqs. (5,6). In both cases, we choose $\varphi_2 = \pi/4$, which implies that $z_2 = w_2$ and consequently $H_0 = 0$. Then, in order to satisfy the fine-tuning condition in Eq. (12), for the first sample network we set $\varphi_1 = \pi/4$. With these choices, after rescaling the linear hopping, Eq. (7) reads

$$\begin{aligned} i\dot{a}_n &= a_{n+1} + a_{n-1} + b_{n+1} - b_{n-1} + U a_n |a_n|^2, \\ i\dot{b}_n &= -b_{n+1} - b_{n-1} - a_{n+1} + a_{n-1} + U b_n |b_n|^2, \end{aligned} \quad (14)$$

and the lattice profile is shown in Fig. 2(a1). For $U = 0$, Eq. (14) has two flatbands at $E_{1,2} = \pm 2$ with the respective CLSs shown in Fig. 2(a2)-(a3). We will refer to this model as *model A*.

For the second sample network we set $\varphi_1 = \pi/6$ - hence fine-tuning condition (12) is not satisfied. Equation (7) after rescaling the linear hopping reads

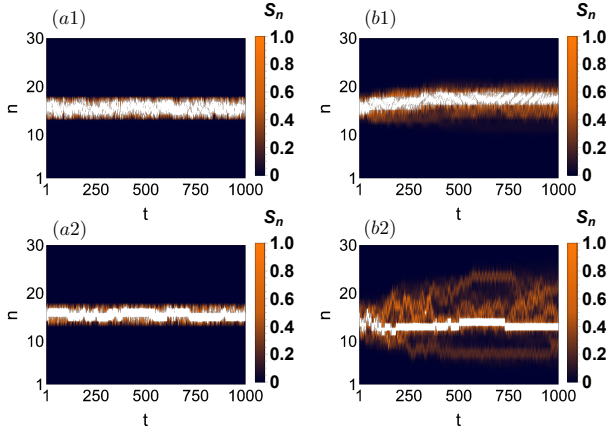
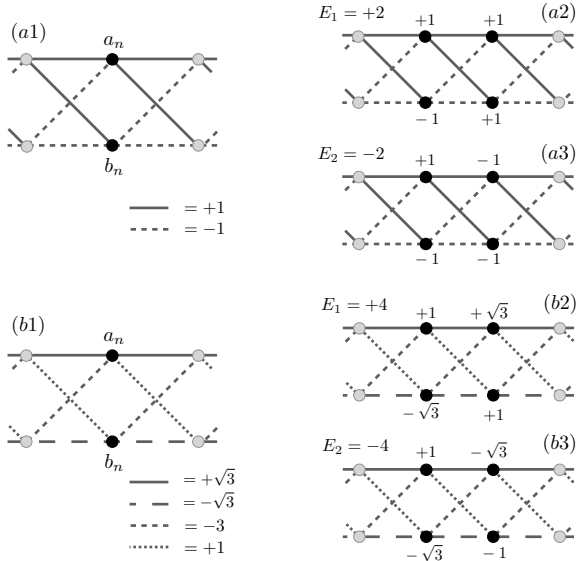
$$\begin{aligned} i\dot{a}_n &= \sqrt{3}a_{n+1} + \sqrt{3}a_{n-1} + b_{n+1} - 3b_{n-1} + U a_n |a_n|^2, \\ i\dot{b}_n &= -\sqrt{3}b_{n+1} - \sqrt{3}b_{n-1} - 3a_{n+1} + a_{n-1} + U b_n |b_n|^2, \end{aligned} \quad (15)$$

and the lattice profile is shown in Fig. 2(b1). For $U = 0$, Eq. (15) has two flatbands at $E_{1,2} = \pm 4$ with the respective CLSs shown in Fig. 2(b2)-(b3). We will refer to this model as *model B*. In Appendix B3 and Appendix B4 we report the rotated equations of these two models, which confirm that the former (model A) has no fully nonlocal terms, while the latter (model B) does.

We visualize the presence (respectively absence) of nonlinear caging in these models by numerically computing their time evolution using symplectic integration schemes - see Appendix B5. We consider a sample compact excitation IC_1 spanning over two unit cells, and we evolve the local density $S_n = |a_n|^2 + |b_n|^2$. The results are shown in Fig. 3 for both models A (14) and B (15) and for two interaction strengths $U = 1$ and $U = 5$. For model A, Eq. (14) - panels (a1)-(a2) - the initial compact excitation IC_1 remains confined within four unit cells, confirming the expected nonlinear caging. For model B, Eq. (15) - panels (b1)-(b2) - the initial excitation is propagating into the chain, confirming that caging is lost.

In Fig. 4 we show the time evolution of the second moment μ_2 defined as

$$\mu_2 = \sum_{n=1}^N [(X - n)^2 (|a_n|^2 + |b_n|^2)] \quad (16)$$



with $X = \sum_{n=1}^N [n(|a_n|^2 + |b_n|^2)]$ for the non-cage preserving model B, Eq. (15). These curves have been averaged over an ensemble of 48 compact initial conditions spanning over two unit cells all chosen with a given total norm $S = \sum_n S_n$ – see details in Appendix B 5. We observe a subdiffusive spreading regime: Within the studied time-window our data agree semi-quantitatively with $\mu_2 \sim t^{0.5}$ for various values of the interaction strength U . The details of this process and its relation to the better studied cases of nonlinear destruction of Anderson localization [5] is certainly an interesting future project. We can only conjecture here that subdiffusion (instead of normal diffusion or even ballistic transport) results from weak interactions renormalizing the CLS and inducing nonlinear

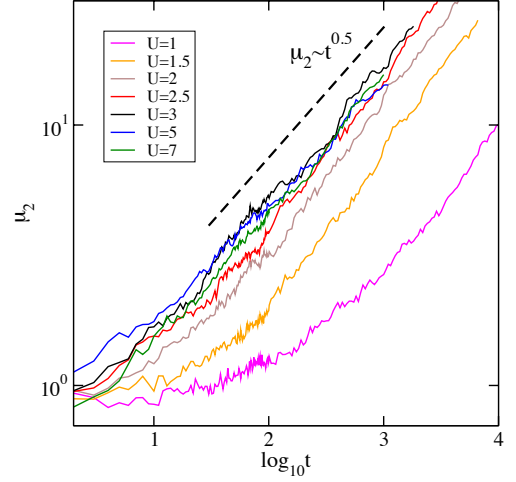


FIG. 4. (Color online) Time-evolution of the second moment μ_2 over an ensemble of 48 initial conditions according to model B, Eq. (15) with $N = 40$ for different U .

interactions between them. Both effects are proportional to the effective interaction strength which decreases with further spreading of the wave packet. Qualitatively this would correspond to a spreading wave packet in an Anderson localization setting where the disorder strength is reduced at the same pace at which the packet spreads.

IV. HUBBARD INTERACTIONS, DELOCALIZATION AND SIGNATURES OF QUANTUM CAGING

Let us now consider interacting bosons evolving on the $\nu = 2$ ABF network parametrized via Eqs. (5,6). We consider the Bose-Hubbard Hamiltonian $\hat{\mathcal{H}}_B = \hat{\mathcal{H}}_0^B + \hat{\mathcal{H}}_1^B$ with

$$\hat{\mathcal{H}}_0^B = - \sum_{n \in \mathbb{Z}} \left[\frac{1}{2} (\hat{c}_n^{\dagger T} H_0 \hat{c}_n) + (\hat{c}_n^{\dagger T} H_1 \hat{c}_{n+1}) + h.c. \right], \quad (17)$$

$$\hat{\mathcal{H}}_1^B = \frac{U}{2} \sum_{n \in \mathbb{Z}} \left[\hat{a}_n^{\dagger} \hat{a}_n^{\dagger} \hat{a}_n \hat{a}_n + \hat{b}_n^{\dagger} \hat{b}_n^{\dagger} \hat{b}_n \hat{b}_n \right]. \quad (18)$$

The annihilation $\hat{c}_n = (\hat{a}_n, \hat{b}_n)$ and creation operators $\hat{c}_n^{\dagger} = (\hat{a}_n^{\dagger}, \hat{b}_n^{\dagger})$ respect the commutation relations $[\hat{a}_n, \hat{a}_k^{\dagger}] = \delta_{n,k}$, $[\hat{b}_n, \hat{b}_k^{\dagger}] = \delta_{n,k}$, and $[\hat{a}_n, \hat{b}_k^{\dagger}] = 0$ for any $n, k \in \mathbb{Z}$. We remark that Eq. (1) follows from $i\partial_t |\Psi\rangle = \hat{\mathcal{H}}_B |\Psi\rangle$ in the single-particle case $U = 0$, by expanding the wave function as $|\Psi\rangle = \sum_n [\psi_{n,1} \hat{a}_n^{\dagger} + \psi_{n,2} \hat{b}_n^{\dagger}] |0\rangle$ for the complex numbers $\psi_{n,1}, \psi_{n,2}$.

A. Delocalization of quantum interacting particles

We now show that interacting bosons break the single particle caging regardless of their number. We focus

networks with the fine-tuned constraint $|w_1|^2 = |z_1|^2$ in Eq. (12) (condition for nonlinear caging) since it straightforward to see the breaking of caging for the other non fine-tuned cases. The Hamiltonian $\hat{\mathcal{H}}_1^B$ in Eq. (18) recast via the transformations U_1 and T in Eqs. (3,4) and represented in terms of the annihilation and creation operators (\hat{p}_n, \hat{f}_n) and $(\hat{p}_n^\dagger, \hat{f}_n^\dagger)$ reads (see Appendix C)

$$\begin{aligned} \hat{\mathcal{H}}_1^B = U \sum_n \bigg\{ & |z_1|^4 \left[\hat{p}_n^\dagger \hat{p}_n^\dagger \hat{p}_n \hat{p}_n + \hat{f}_n^\dagger \hat{f}_n^\dagger \hat{f}_n \hat{f}_n \right] \\ & + 4|z_1|^4 \hat{p}_n^\dagger \hat{f}_{n+1}^\dagger \hat{p}_n \hat{f}_{n+1} \\ & + z_1^{*2} w_1^2 \hat{p}_n^\dagger \hat{p}_{n+1}^\dagger \hat{f}_{n+1} \hat{f}_{n+1} + z_1 w_1^{*2} \hat{p}_n \hat{p}_{n+1} \hat{f}_{n+1}^\dagger \hat{f}_{n+1}^\dagger \bigg\}. \end{aligned} \quad (19)$$

Let us consider those terms located in the bottom line of both Eq. (13) and Eq. (19) - respectively shown in Fig. 5 (a) and (b). Both sets of terms link the decoupled single particle dimers (solid gray lines). However, for the classical terms $\hat{p}_n^2 \hat{f}_{n+1}^{*2} + \text{h.c.}$ to be nonzero the densities on both sites have to be nonzero. Instead the quantum terms $\hat{p}_n \hat{p}_{n+1} \hat{f}_{n+1}^\dagger \hat{f}_{n+1}^\dagger + \text{h.c.}$ apply as soon as two bosons access one of the two sites - irrespective of the presence of particles on the other site. The classical term is a density-density interaction, while the quantum one provides coherent transport for pairs of particles [35]. Hence, even if we consider an arbitrary number of bosons initially located within a finite portion of the system in a compact distribution, such interaction terms in general will allow pairs of particles to propagate along the network breaking the initial confinement. Yet, the fine-tuned quantum system via Eq. 12 does carry quantum caging eigenstates, as we will show below.

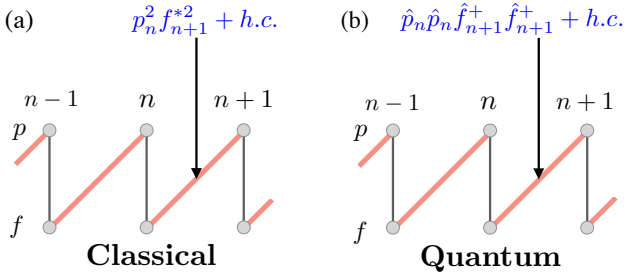


FIG. 5. (Color online) Schematic representation of linear hopping (solid gray lines) and interaction terms (red shaded lines) for the classical nonlinear case (a) and the quantum Hubbard case (b).

B. Signatures of quantum caging

We study the propagation of two interacting particles (TIP) initially located at the same site at the center of the network. For convenience and without loss of generality, we consider distinguishable bosons. We compute the time-evolution of their wave-function $|\Psi\rangle$ which is governed by a two-dimensional Schrödinger system whose

coordinates (n, k) represent the spatial position of each boson. We consider a network for $N = 40$ unit cells and compute the local density $\rho_{n,k}$ of the two particles and the correspondent one-dimensional probability distribution function (PDF) of the particle density defined as $Q_n = \sum_{k=1}^N \rho_{n,k}$ - details and definitions are provided in Appendix D. As the underlying networks, we consider the same sample geometries studied in Sec. IIIB - with the single particle (linear) terms defined in Eq. (14) (model A) and Eq. (15) (model B) - since the former satisfies the nonlinear caging condition in Eq. (12) while the latter does not.

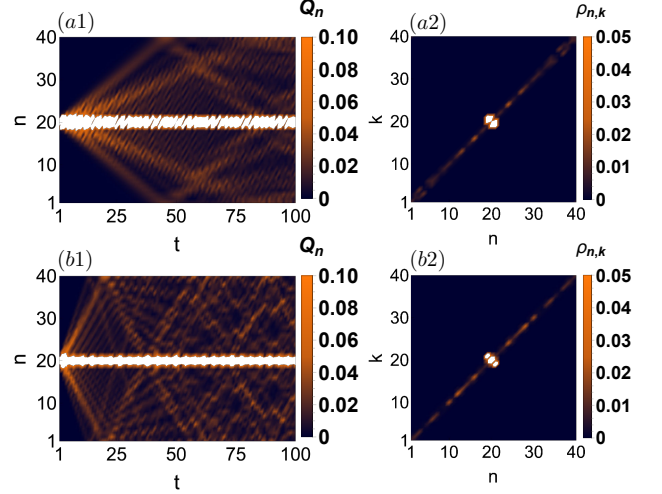


FIG. 6. (Color online) Model A - where the linear network defined in Eq. (14) satisfies the nonlinear caging condition Eq. (12). (a1) Time evolution of Q_n and (b1) local density $\rho_{n,k}$ at time $t = 100$, both with $U = 1$. (a2-b2) Same (a1-b1) for $U = 5$.

In Fig. 6 (a1-b1) we plot the time-evolution of Q_n for the first sample geometry in Eq. (14) for two interaction strengths $U = 1$ (top) and $U = 5$ (bottom) respectively. Both cases show that a part of the PDF is propagating ballistically - indicating the spreading of the particles along the network, destroying single particle caging. Simultaneously, we observe that a substantial portion of Q_n remains localized around the $n = \frac{N}{2}$ unit cell (initial location of both particles). This is further detailed in Fig. 6 (a2-b2), where we plot the local density $\rho_{n,k}$ at time $t = 100$ for $U = 1$ and $U = 5$ respectively. Firstly, these panels show that the delocalization and ballistic spreading of a part of the wave-function $|\Psi\rangle$ occurs along the diagonal $n = k$ of the Schrödinger system, which indicates that the particles have to stay in a bound state in order to delocalize. Secondly, jointly with the extended wave along the diagonal $k = n$, these plots show a large amplitude density peak at the original launching site. Such longstanding localized strong excitations indicate that there exist non-propagating spatially compact states which have been excited by placing both particles initially in the same cell, and these states ensure nontriv-

ial caging of interacting particles. The existence and the properties of these states will be discussed in a forthcoming work [34].

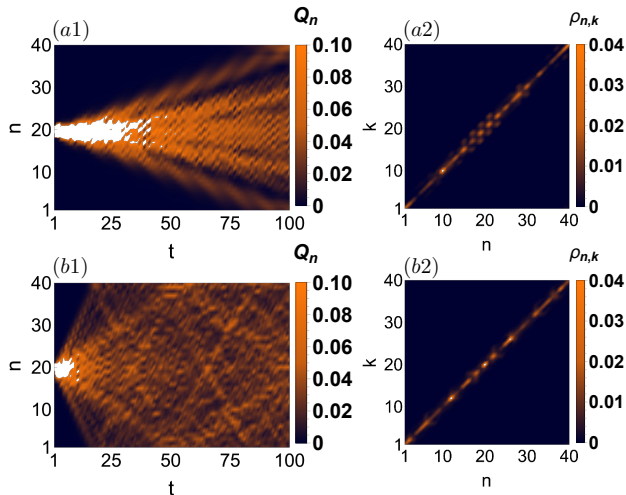


FIG. 7. (Color online) Model B - where the linear network defined in Eq. (15) does not satisfy the nonlinear caging condition Eq. (12). (a1) Time evolution of Q_n and (b1) local density $\rho_{n,k}$ at time $t = 100$, both with $U = 1$. (a2-b2) Same (a1-b1) for $U = 5$.

The signatures of quantum caging are absent for an underlying linear geometry which does not obey the fine-tuning condition Eq. (12). Indeed, in Fig. 7 (a1-b1) we show the time-evolution of Q_n for the second sample geometry, model B (15) for $U = 1$ (top) and $U = 5$ (bottom) respectively. These plots again show ballistic spreading, i.e. the existence of spatially extended bound states. However, no considerable localized fraction of the PDF Q_n is observed. This is also confirmed in Fig. 7 (a2-b2), where the local density $\rho_{n,k}$ at time $t = 100$ is shown for $U = 1$ and $U = 5$ respectively.

V. DISCUSSIONS AND PERSPECTIVES

In this work we studied the impact of classical and quantum interactions in lattices without linear dispersion. We showed that in one dimension all compact localized states can be completely detangled via unitary transformations – a fact that yields a systematic generator for all band flat networks with finite-range hopping terms [9]. We used two bands networks as testbeds to show that single particle caging is in general broken by both classical and quantum interactions.

At the same time caging survives when specific fine-tuning conditions of the single particle Hamiltonian are satisfied. In the classical case these fine-tuning conditions ensure that spatially compact initial excitations states remain compact at all times. In the quantum case the picture is more complex. Our study of two interacting particles highlighted that Hubbard interactions simulta-

neously produce coherently transporting eigenstates as well as compact localized eigenstates. These latter states are macroscopically degenerate, and at variance with the product states of noninteracting single particle CLS their energies are renormalized by the interaction strength. These features will be discussed in the subsequent part of this work [34]: As we will show, the existence of these renormalized compact states extends to any finite number $2 \leq M < \infty$ of interacting particles evolving on an infinite lattice $N \rightarrow \infty$. These novel types of compact states of interacting particles extend the notion of single particle compact states that exist in flatband lattices [7, 8]. There is therefore room for future studies, ranging from $d = 1$ systems with larger number of bands $\nu \geq 3$ - where *e.g.* these very questions have been approached for a specific three band problem (the rhombic (diamond) chain with fine-tuned magnetic field, see Refs. [31–33]) - to higher dimensional networks and even lattices with both flat and dispersive bands [36].

An important merit of fine-tuning is its subsequent detuning. Flatband models are fine-tuned submanifolds of suitably defined spaces of Hamiltonian functions. Further fine-tuning render all the bands flat and yield sub-submanifolds of ABF lattices. These Hamiltonians are in general sensitive to perturbations like interactions, and our results show that cage-preserving ABF lattices form additionally fine-tuned structures within the ABF sub-submanifolds. These structures - proper of the Hubbard interaction - may substantially change when adding tunability to interaction Hamiltonian terms, for example leading to many-body flatband localization [37]. Unfolding the details of these various layers of fine-tuned submanifolds, and the impact of perturbations – *e.g.* disorder, dissipation, among others – is a thrilling field of future research.

VI. ACKNOWLEDGMENTS

The authors thank Ihor Vakulchyk and Ajith Ramachandran for helpful discussions. This work was supported by the Institute for Basic Science, Korea (IBS-R024-D1).

Appendix A: Detangling of dispersionless networks

1. Proof

We provide in this section the technical details of the proof that any $d = 1$ all bands flat Hamiltonian with finite-range hopping is equivalent to a set of decoupled sites up to a unitary transformation. Equivalently, in $d = 1$ short-range ABF Hamiltonians only have compact localised states of size/class $u = 1$. The core assumption of the proof is that the eigenstates of flatbands of such a Hamiltonian can be represented as compact localised states. All the known examples of $d = 1$ flat-

bands with finite-range hopping support this observation. This immediately constraints the possible eigenstates of the Bloch Hamiltonian, and as we will see this constraint together with the finite-range hopping condition turns out to be enough to enforce the result. We will use the $\langle A, B \rangle$ to denote the scalar product of matrices: $\langle A, B \rangle = \text{Tr}(A^\dagger B)$ or vectors $\langle A, B \rangle = \sum_a A_a^* B_a$ throughout this appendix.

Let's consider a $d = 1$ ν band Hamiltonian with all bands flat. We assume that all of its eigenstates can be represented as CLS of size $u \leq \nu$ (in case of flatbands with CLS of different size, we assume that they are all padded by zeros to the size of the largest one). This implies that the corresponding Bloch eigenstates take the following form (up to normalisation prefactor, that still depends on the wavevector q):

$$\Psi_{\alpha,a}(q) = \frac{\sum_{b=0}^{u-1} C_{\alpha,ab} \omega_{qb}}{\sqrt{\langle C_{\alpha}\omega_q, C_{\alpha}\omega_q \rangle}} \propto \sum_{b=0}^{u-1} C_{\alpha,ab} e^{ibq}, \quad (\text{A1})$$

$$\omega_q = (1, e^{iq}, \dots, e^{iq(u-1)}), \quad (\text{A2})$$

where α is the band index, a is the wavefunction component. The $\nu \times u$ matrix C_α is parameterising the CLS of band α , and the central object of all the following derivations. The eigenstates of a Hermitian Hamiltonian have to be orthogonal, giving the first set of constraints on the matrices C_α :

$$\delta_{\alpha\beta} = \sum_a \Psi_{\alpha,a}^*(q) \Psi_{\beta,a}(q) \propto \sum_{abc} e^{iq(c-b)} C_{\alpha,ab}^* C_{\beta,ac} = \sum_{bc} e^{iq(c-b)} T_{\alpha\beta,bc}. \quad (\text{A3})$$

We have defined the $\nu \times \nu$ matrices $T_{\alpha\beta} = \langle C_\alpha, C_\beta \rangle$, that will be used later. The above orthogonality condition reduces to a specific Fourier transform of the matrices $T_{\alpha\beta}$, which implies that the matrices $T_{\alpha\beta}$, $\alpha \neq \beta$ have to have zero sums over any diagonal.

Using this parameterisation of the eigenstates, we can use the spectral decomposition to reconstruct the Hamiltonian itself:

$$\begin{aligned} \mathcal{H}_q &= M_q \Lambda M_q^\dagger \quad \Lambda_{ab} = \varepsilon_a \delta_{ab}, \\ M_q &= (\Psi_1 \Psi_2 \dots \Psi_\nu), \\ \Psi_{\alpha,a} &= \frac{C_{\alpha}\omega_q}{\sqrt{\langle C_{\alpha}\omega_q, C_{\alpha}\omega_q \rangle}}. \end{aligned} \quad (\text{A4})$$

The Hamiltonian becomes:

$$\mathcal{H}_q = \sum_\alpha \varepsilon_\alpha \frac{(C_\alpha \omega_q) \otimes (C_\alpha \omega_q)^*}{\langle C_\alpha \omega_q, C_\alpha \omega_q \rangle}.$$

Here, $P_\alpha(q) = (C_\alpha \omega_q) \otimes (C_\alpha \omega_q)^*$ and $Q_\alpha(q) = \langle C_\alpha \omega_q, C_\alpha \omega_q \rangle$ are polynomials in e^{iq} of degree $u-1$ and degree at most $u-1$ respectively, and every term in the above sum is their ratio. Therefore the Hamiltonian is long-ranged in general. The above Hamiltonian becomes

short-ranged iff P_α is divisible by $Q_\alpha \forall \alpha$. If the degree of Q_α is $u-1$ the ratio P_α/Q_α is a constant, the respective eigenvector is q -independent and the CLS is of class $u=1$. Since they are already of class $u=1$, these eigenvalues can be excluded, for example by considering only an orthogonal subspace of the Hilbert space. Therefore I assume that the degree of $Q_\alpha(q)$ is at most $u-2$ in general. This implies that $T_{\alpha\alpha,1U} = T_{\alpha\alpha,U1} = 0$ always (see Eq. (A3)). The lower the degree of Q_α the more zero sum diagonals do $T_{\alpha\alpha}$ have, starting from the corners. Combining this statement with the earlier result that diagonals of $T_{\alpha\beta}$ sum up to zero we see that the amplitudes in the first unit cell of any CLS are always orthogonal to the amplitudes in the last unit cell of any CLS. As we will see below this is the cornerstone of the proof of the triviality of the all bands flat Hamiltonians in $d=1$.

To reconstruct the Hamiltonian we need to find the matrices C_α . This requires a solution of a system of coupled matrix quadratic equations with respect to C_α , $\alpha = 1, \dots, \nu$:

$$\langle C_\alpha, C_\beta \rangle = T_{\alpha\beta},$$

considering $T_{\alpha\beta}$ as input parameters. The solution can be constructed sequentially: we parameterise $C_\alpha = (c_{\alpha 1}, c_{\alpha 2}, \dots, c_{\alpha u})$, where $c_{\alpha a}$ is a vector of the eigenfunction amplitudes in the unit cell a of the CLS of the band α . This transforms the above equations into a set of coupled quadratic equations for $c_{\alpha a}$. We solve these equations iteratively by fixing $c_{\alpha,a}$ one by one starting from $\alpha=1$ and only taking into account the equations involving $\beta \leq \alpha$. We also employ extensively our freedom in the choice of the basis vector of the Hilbert space, to simplify the solution. The core idea is to see how the equations constrain the possible shapes of $c_{\alpha,1}$ and $c_{\alpha,\nu}$ and show that one can always redefine the unit cell to reduce the sizes of all the CLS by 1.

We start by setting $c_{11} = e_1$ - this defines the first basis vector. Then $T_{11,1u} = 0$ implies that we can define $c_{1u} = e_2$. For c_{21} we have the following constraint:

$$T_{12,u1} = \langle c_{1u}, c_{21} \rangle = 0,$$

and we can choose $c_{21} = *e_1 + *e_3$, where we defined the next basis vector e_3 and the asterisks stand for some (possibly zero) coefficients. The c_{2u} is constrained by

$$T_{21,1u} = \langle c_{11}, c_{2u} \rangle = 0,$$

$$T_{22,1u} = \langle c_{21}, c_{2u} \rangle = 0.$$

The most generic form of $c_{2u} = *e_2 + *e_4$ - again defining the basis vector e_4 . Such incremental construction enforces $c_{\beta U}$ to have zeros at positions where $c_{\alpha 1}$ has non-zero elements and vice versa. It therefore guarantees the existence of a pattern of non-zero elements in C_α that is the same $\forall \alpha$.

We illustrate this result by a specific case of $\nu=3$, $U=3$ (there is a single possible redefinition of the unit cell in the case of $\nu=2$ and $u=2$, that we discuss in

the next appendix): working out the matrices C_1, C_2, C_3 following the above rules we find:

$$C_1 = \begin{pmatrix} * & * & 0 \\ 0 & * & * \\ 0 & * & 0 \end{pmatrix}, C_2 = \begin{pmatrix} * & * & 0 \\ 0 & * & * \\ * & * & 0 \end{pmatrix}, C_3 = \begin{pmatrix} * & * & 0 \\ 0 & * & * \\ * & * & 0 \end{pmatrix}.$$

As before the asterisks $*$ denote unspecified coefficients. The shape of the all the matrices supports a redefinition of the unit cell, that reduces the sizes of all the CLS/matrices to $u = 2$.

2. Parametrization of $\nu = 2$ networks

The above proof when inverted yields a generator scheme for dispersionless networks. In this subsection, we explicitly unfold the two bands problem, $\nu = 2$. Let us consider a non-degenerate (two different flat-band energies) fully decoupled network in coordinates $\phi_n = (\alpha_n, \beta_n)$.

$$i\dot{\phi}_n = -H_0^{(1)}\phi_n - H_1^{(1)}\phi_{n+1} - H_1^{(1)\dagger}\phi_{n-1}, \quad (\text{A5})$$

$$H_0^{(1)} = \begin{pmatrix} -1 & 0 \\ 0 & 1 \end{pmatrix} \quad H_1^{(1)} = \begin{pmatrix} 0 & 0 \\ 0 & 0 \end{pmatrix}, \quad (\text{A6})$$

with two flatband energies $E_1 = -1$ and $E_2 = 1$. The mapping in Eq. (3) consists of two unitary transformations U_1 and U_2 , which are parametrized as

$$U_i = e^{i\theta_i} \begin{pmatrix} z_i & w_i \\ -w_i^* & z_i^* \end{pmatrix} \quad i = 1, 2 \quad (\text{A7})$$

by the complex numbers z_i, w_i such that $|z_i|^2 + |w_i|^2 = 1$ and the phases θ_i . The unit cell redefinition T is

$$T: \begin{cases} p_n \mapsto p_n \\ f_n \mapsto f_{n-1} \end{cases} \quad (\text{A8})$$

We generate all the $\nu = 2$ dispersionless lattices by applying the transformations, Eqs. (A7,A8) in the following order

$$\begin{pmatrix} \alpha_n \\ \beta_n \end{pmatrix} \xrightarrow{U_2} \begin{pmatrix} p_n \\ f_n \end{pmatrix} \xrightarrow{T} \begin{pmatrix} p_n \\ f_n \end{pmatrix} \xrightarrow{U_1} \begin{pmatrix} a_n \\ b_n \end{pmatrix}, \quad (\text{A9})$$

as shown in Fig. 8.

The first coordinate rotation U_2 turns $H_0^{(1)}$ in Eq. (A6) to

$$H_0^{(2)} = U_2 H_0^{(1)} U_2^\dagger = \begin{pmatrix} |w_2|^2 - |z_2|^2 & 2z_2 w_2 \\ 2z_2^* w_2^* & |z_2|^2 - |w_2|^2 \end{pmatrix}, \quad (\text{A10})$$

while $H_1^{(2)} = U_2 H_1^{(1)} U_2^\dagger$ remains zero - as shown in Fig. 8(a1), right plot.

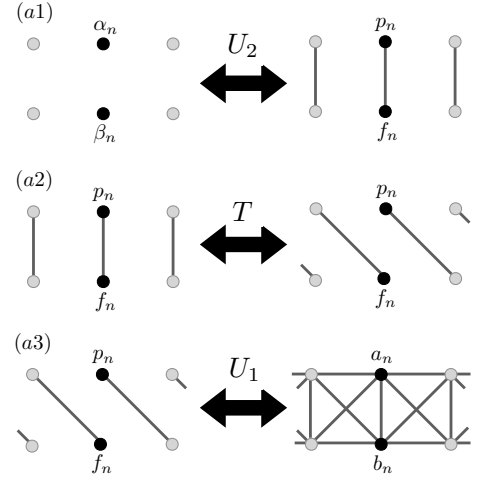


FIG. 8. (Color online) Schematic representation of the unit cell redefinition for $\nu = 2$ bands lattice. In each panel, the black dots represent the chosen unit cell.

The unit cell redefinition T in Eq. (A8) redefines $H_0^{(2)}$ and $H_1^{(2)}$ as

$$H_0^{(3)} = \begin{pmatrix} |w_2|^2 - |z_2|^2 & 0 \\ 0 & |z_2|^2 - |w_2|^2 \end{pmatrix}, \quad (\text{A11})$$

$$H_1^{(3)} = \begin{pmatrix} 0 & 2z_2 w_2 \\ 0 & 0 \end{pmatrix}, \quad (\text{A12})$$

as shown in Fig. 8(a2), right plot.

At last, the rotation U_1 turns $H_0^{(3)}$ and $H_1^{(3)}$ in Eqs. (A11,A12) to the following matrices

$$H_0 = U_1 H_0^{(3)} U_1^\dagger = \Gamma_0 \begin{pmatrix} |z_1|^2 - |w_1|^2 & -2z_1 w_1 \\ -2z_1^* w_1^* & |w_1|^2 - |z_1|^2 \end{pmatrix}, \quad (\text{A13})$$

$$H_1 = U_1 H_1^{(3)} U_1^\dagger = \Gamma_1 \begin{pmatrix} z_1 w_1^* & z_1^2 \\ -(w_1^*)^2 & -z_1 w_1^* \end{pmatrix}, \quad (\text{A14})$$

for $\Gamma_0 = |w_2|^2 - |z_2|^2$ and $\Gamma_1 = 2z_2 w_2$ - as shown in Fig. 8(a3), right plot.

Appendix B: Detangling procedure applied to nonlinear dispersionless models

In this appendix, we apply the detangling procedure as described by Eq. (3) to the dispersionless, two band models in presence of a local Kerr nonlinearity (9).

1. Preserving the caging in $\nu = 2$ networks: a necessary and sufficient condition

We now work out the detangled local Kerr nonlinearity for a general $\nu = 2$ ABF lattice. The transformation U_1

in components read

$$U_1 : \begin{cases} a_n = e^{i\theta_1}(z_1 p_n + w_1 f_n) \\ b_n = e^{i\theta_1}(-w_1^* p_n + z_1^* f_n) \end{cases} \quad (\text{B1})$$

Via Eq. (B1), the nonlinear terms turn

$$\begin{aligned} a_n |a_n|^2 &= e^{i\theta_1} [z_1 |z_1|^2 p_n |p_n|^2 + z_1^2 w_1^* p_n^2 f_n^* \\ &\quad + z_1^* w_1^2 p_n^* f_n^2 + w_1 |w_1|^2 f_n |f_n|^2 \\ &\quad + 2|z_1|^2 w_1 |p_n|^2 f_n + 2z_1 |w_1|^2 p_n |f_n|^2], \\ b_n |b_n|^2 &= e^{i\theta_1} [-w_1^* |w_1|^2 p_n |p_n|^2 + z_1 w_1^{*2} p_n^2 f_n^* \\ &\quad - z_1^{*2} w_1 p_n^* f_n^2 + z_1^* |z_1|^2 f_n |f_n|^2 \\ &\quad + 2z_1^* |w_1|^2 |p_n|^2 f_n - 2|z_1|^2 w_1^* p_n |f_n|^2]. \end{aligned} \quad (\text{B2})$$

The equations for p_n then read

$$\begin{aligned} i\dot{p}_n &= -(|z_2|^2 - |w_2|^2)p_n + 2w_2 z_2 f_{n-1} \\ &\quad + e^{i\theta_1} U \{ (|z_1|^4 + |w_1|^4) p_n |p_n|^2 \\ &\quad + 2z_1^{*2} w_1^2 p_n^* f_{n-1}^2 + 4|z_1|^2 |w_1|^2 p_n |f_{n-1}|^2 \\ &\quad + z_1 w_1^* (|z_1|^2 - |w_1|^2) p_n^2 f_{n-1}^* \\ &\quad + z_1^* w_1 (|w_1|^2 - |z_1|^2) f_{n-1} |f_{n-1}|^2 \\ &\quad + 2z_1^* w_1 (|z_1|^2 - |w_1|^2) |p_n|^2 f_{n-1} \}. \end{aligned} \quad (\text{B3})$$

The unit cell redefinition $f_n \mapsto f_{n-1}$ yields the "fully nonlocal" terms $f_{n-1} |f_{n-1}|^2$

$$\begin{aligned} i\dot{p}_n &= -(|z_2|^2 - |w_2|^2)p_n + 2w_2 z_2 f_n \\ &\quad + e^{i\theta_1} U \{ (|z_1|^4 + |w_1|^4) p_n |p_n|^2 \\ &\quad + 2z_1^{*2} w_1^2 p_n^* f_{n-1}^2 + 4|z_1|^2 |w_1|^2 p_n |f_{n-1}|^2 \\ &\quad + z_1 w_1^* (|z_1|^2 - |w_1|^2) p_n^2 f_{n-1}^* \\ &\quad + z_1^* w_1 (|w_1|^2 - |z_1|^2) f_{n-1} |f_{n-1}|^2 \\ &\quad + 2z_1^* w_1 (|z_1|^2 - |w_1|^2) |p_n|^2 f_{n-1} \} \end{aligned} \quad (\text{B4})$$

which break the caging effect. These terms are not present if $|w_1|^2 = |z_1|^2$, which reduces Eq. (B4) to

$$\begin{aligned} i\dot{p}_n &= -(|z_2|^2 - |w_2|^2)p_n + 2w_2 z_2 f_n \\ &\quad + 2e^{i\theta_1} U \{ |z_1|^4 (p_n |p_n|^2 + 2p_n |f_{n-1}|^2) + z_1^{*2} w_1^2 p_n^* f_{n-1}^2 \}. \end{aligned} \quad (\text{B5})$$

Similarly follows for f_n

$$\begin{aligned} i\dot{f}_n &= (|z_2|^2 - |w_2|^2)f_n + 2w_2^* z_2^* p_{n+1} \\ &\quad + e^{i\theta_1} U \{ (|z_1|^4 + |w_1|^4) f_n |f_n|^2 + \\ &\quad + 2z_1^2 w_1^{*2} p_n^2 f_n^* + 4|z_1|^2 |w_1|^2 |p_n|^2 f_n \\ &\quad + z_1^* w_1 (|w_1|^2 - |z_1|^2) p_n^2 f_n^* \\ &\quad + z_1 w_1^* (|z_1|^2 - |w_1|^2) f_n |f_n|^2 \\ &\quad + 2z_1 w_1^* (|w_1|^2 - |z_1|^2) |p_n|^2 f_n \}, \end{aligned} \quad (\text{B6})$$

which after the unit cell redefinition $f_n \mapsto f_{n-1}$ and enforcement of the condition $|w_1|^2 = |z_1|^2$ reduces to

$$\begin{aligned} i\dot{f}_n &= (|z_2|^2 - |w_2|^2)f_n + 2w_2^* z_2^* p_n \\ &\quad + 2e^{i\theta_1} U \{ |z_1|^4 (f_n |f_n|^2 + 2|p_{n+1}|^2 f_n) + z_1^2 w_1^{*2} p_{n+1}^2 f_n^* \}. \end{aligned} \quad (\text{B7})$$

As a result we observe the following:

1. the condition $|w_1|^2 = |z_1|^2$ in Eq. (A7) is *necessary* to preserve the caging - otherwise "fully nonlocal" terms which break the caging exist in Eq. B4 - and it is *sufficient* - since the subsequent transformation by U_2 in Eq. (A7) will not introduce additional "fully nonlocal" terms.
2. the condition $|w_1|^2 = |z_1|^2$ in Eq. (A7) yields all the entrees of the matrix H_1 in Eq. (A14) have equal magnitude in absolute value.

2. Rotating the classical interaction Hamiltonian \mathcal{H}_1^G

Collecting together the rotated Eqs. (B5,B7) of a dispersionless $\nu = 2$ nonlinear network under the condition $|w_1|^2 = |z_1|^2$ in transformation U_1 (A7) we find

$$\begin{aligned} i\dot{p}_n &= |w_2|^2 p_n + w_2 z_2 f_n \\ &\quad + 2U \{ |z_1|^4 (p_n |p_n|^2 + 2p_n |f_{n+1}|^2) + z_1^{*2} w_1^2 p_n^* f_{n+1}^2 \}, \\ i\dot{f}_n &= |z_2|^2 f_n + w_2 z_2^* p_n \\ &\quad + 2U \{ |z_1|^4 (f_n |f_n|^2 + 2|p_{n-1}|^2 f_n) + z_1^2 w_1^{*2} p_{n-1}^2 f_n^* \}. \end{aligned} \quad (\text{B8})$$

These equations are the equations of motion $i\dot{p}_n = \frac{\partial \mathcal{H}_G}{\partial p_n^*}$ and $i\dot{f}_n = \frac{\partial \mathcal{H}_G}{\partial f_n^*}$ of the Hamiltonian \mathcal{H}_G

$$\mathcal{H}_G = \mathcal{H}_0^G + \mathcal{H}_1^G, \quad (\text{B9})$$

where

$$\mathcal{H}_0^G = \sum_n \{ -|w_2|^2 |p_n|^2 - |z_2|^2 |f_n|^2 - w_2 z_2 (p_n^* f_n + p_n f_n^*) \}, \quad (\text{B10})$$

and

$$\begin{aligned} \mathcal{H}_1^G &= U \sum_n \{ |z_1|^4 [|p_n|^4 + |f_n|^4 + 4|p_n|^2 |f_{n+1}|^2] \\ &\quad + z_1^{*2} w_1^2 p_n^2 f_{n+1}^2 + z_1 w_1^{*2} p_n^2 f_{n+1}^* \}. \end{aligned} \quad (\text{B11})$$

Below we generate specific models by setting $z_i = \cos \varphi_i$, $w_i = \sin \varphi_i$ and $\theta_i = 0$ in the transformations $U_{i=1,2}$ (A7).

3. Model A

This model

$$\begin{aligned} i\dot{a}_n &= a_{n+1} + a_{n-1} + b_{n+1} - b_{n-1} + U a_n |a_n|^2 \\ i\dot{b}_n &= -b_{n+1} - b_{n-1} - a_{n+1} + a_{n-1} + U b_n |b_n|^2 \end{aligned} \quad (\text{B12})$$

is obtained by choosing $\varphi_1 = \varphi_2 = \pi/4$ in transformations $U_{1,2}$ (4)/(A7):

$$U_1 : \begin{cases} p_n = \frac{a_n + b_n}{\sqrt{2}} \\ f_n = \frac{a_n - b_n}{\sqrt{2}} \end{cases} \Leftrightarrow \begin{cases} a_n = \frac{p_n + f_n}{\sqrt{2}} \\ b_n = \frac{p_n - f_n}{\sqrt{2}} \end{cases} \quad (\text{B13})$$

and

$$U_2 : \begin{cases} \alpha_n = \frac{p_n + f_n}{\sqrt{2}} \\ \beta_n = \frac{p_n - f_n}{\sqrt{2}} \end{cases} \Leftrightarrow \begin{cases} p_n = \frac{\alpha_n + \beta_n}{\sqrt{2}} \\ f_n = \frac{\alpha_n - \beta_n}{\sqrt{2}} \end{cases} \quad (\text{B14})$$

Equations of motion (B12) then read

$$\begin{aligned} i\dot{p}_n &= 2f_{n-1} + \frac{U}{2} [p_n|p_n|^2 + f_n^2 p_n^* + 2p_n|f_n|^2], \\ i\dot{f}_n &= 2p_{n+1} + \frac{U}{2} [f_n|f_n|^2 + p_n^2 f_n^* + 2|p_n|^2 f_n]. \end{aligned} \quad (\text{B15})$$

The unit cell redefinition $f_n \mapsto f_{n-1}$ maps Eq. (B15) to

$$\begin{aligned} i\dot{p}_n &= 2f_n + \frac{U}{2} [p_n|p_n|^2 + f_{n-1}^2 p_n^* + 2p_n|f_{n-1}|^2], \\ i\dot{f}_n &= 2p_n + \frac{U}{2} [f_n|f_n|^2 + p_{n+1}^2 f_n^* + 2|p_{n+1}|^2 f_n]. \end{aligned} \quad (\text{B16})$$

At last, the second transformation U_2 (B14) rotates Eq. (B16) to

$$\begin{aligned} i\dot{\alpha}_n &= 2\alpha_n + \frac{U}{8} \{ \alpha_n|\alpha_n|^2 + \beta_n^2 \alpha_n^* + 2\alpha_n|\beta_n|^2 \\ &\quad + \alpha_n^* \alpha_{n+1}^2 + \alpha_n^* \beta_{n+1}^2 - 2\alpha_n^* \alpha_{n+1} \beta_{n+1} \\ &\quad + \beta_n^* \alpha_{n+1}^2 + \beta_n^* \beta_{n+1}^2 - 2\beta_n^* \alpha_{n+1} \beta_{n+1} \\ &\quad + \alpha_n^* \alpha_{n-1}^2 + \alpha_n^* \beta_{n-1}^2 + 2\alpha_n^* \alpha_{n-1} \beta_{n-1} \\ &\quad - \beta_n^* \alpha_{n-1}^2 - \beta_n^* \beta_{n-1}^2 - 2\beta_n^* \alpha_{n-1} \beta_{n-1} \\ &\quad + 2(\alpha_n|\alpha_{n+1}|^2 - \alpha_n \alpha_{n+1}^* \beta_{n+1} \\ &\quad - \alpha_n \alpha_{n+1} \beta_{n+1}^* + \alpha_n |\beta_{n+1}|^2) \\ &\quad + 2(\beta_n|\alpha_{n+1}|^2 - \alpha_{n+1}^* \beta_n \beta_{n+1} \\ &\quad - \alpha_{n+1} \beta_n \beta_{n+1}^* + \beta_n |\beta_{n+1}|^2) \\ &\quad + 2(\alpha_n|\alpha_{n-1}|^2 + \alpha_n \alpha_{n-1}^* \beta_{n-1} \\ &\quad + \alpha_n \alpha_{n-1} \beta_{n-1}^* + \alpha_n |\beta_{n-1}|^2) \\ &\quad - 2(\beta_n|\alpha_{n-1}|^2 + \alpha_{n-1}^* \beta_n \beta_{n-1} \\ &\quad + \alpha_{n-1} \beta_n \beta_{n-1}^* + \beta_n |\beta_{n-1}|^2) \} \end{aligned} \quad (\text{B17})$$

where only one equation of motion for component α_n is presented for the sake of space. The above equation does not posses any *fully nonlocal* term which depends solely on $\alpha_{n\pm 1}, \beta_{n\pm 1}$, their products or complex conjugates.

4. Model B

This model

$$\begin{aligned} i\dot{a}_n &= \sqrt{3}a_{n+1} + \sqrt{3}a_{n-1} + b_{n+1} - 3b_{n-1} + g a_n |a_n|^2 \\ i\dot{b}_n &= -\sqrt{3}b_{n+1} - \sqrt{3}b_{n-1} - 3a_{n+1} + a_{n-1} + g b_n |b_n|^2 \end{aligned} \quad (\text{B18})$$

is obtained choosing $\varphi_1 = \pi/6$ and $\varphi_2 = \pi/4$ in transformations $U_{1,2}$ (4). The rotation U_2 is then the same as

Eq. (B14), while U_1 reads

$$U_1 : \begin{cases} p_n = \frac{\sqrt{3}a_n + b_n}{2} \\ f_n = \frac{a_n - \sqrt{3}b_n}{2} \end{cases} \Leftrightarrow \begin{cases} a_n = \frac{\sqrt{3}p_n + f_n}{2} \\ b_n = \frac{p_n - \sqrt{3}f_n}{2} \end{cases} \quad (\text{B19})$$

Applying this rotation Eq. (B18) then turns

$$\begin{aligned} i\dot{p}_n &= 4f_{n-1} + \frac{U}{16} [10p_n|p_n|^2 + 2\sqrt{3}p_n^2 f_n^* + 6f_n^2 p_n^* \\ &\quad - 2\sqrt{3}f_n|f_n|^2 + 4\sqrt{3}|p_n|^2 f_n + 12p_n|f_n|^2], \\ i\dot{f}_n &= 4p_{n+1} + \frac{U}{16} [2\sqrt{3}p_n|p_n|^2 + 6p_n^2 f_n^* - 2\sqrt{3}f_n^2 p_n^* \\ &\quad + 10f_n|f_n|^2 + 12|p_n|^2 f_n - 4\sqrt{3}p_n|f_n|^2]. \end{aligned} \quad (\text{B20})$$

The unit cell redefinition $f_n \mapsto f_{n-1}$ maps Eq. (B20) to

$$\begin{aligned} i\dot{p}_n &= 4f_n + \frac{U}{16} [10p_n|p_n|^2 + 2\sqrt{3}p_n^2 f_{n-1}^* \\ &\quad + 6f_{n-1}^2 p_n^* - 2\sqrt{3}f_{n-1}|f_{n-1}|^2 \\ &\quad + 4\sqrt{3}|p_n|^2 f_{n-1} + 12p_n|f_{n-1}|^2], \\ i\dot{f}_n &= 4p_n + \frac{U}{16} [2\sqrt{3}p_{n+1}|p_{n+1}|^2 + 6p_{n+1}^2 f_n^* \\ &\quad - 2\sqrt{3}f_n^2 p_{n+1}^* + 10f_n|f_n|^2 \\ &\quad + 12|p_{n+1}|^2 f_n - 4\sqrt{3}p_{n+1}|f_n|^2]. \end{aligned} \quad (\text{B21})$$

We see here the emergence of "fully nonlocal" terms such as $f_{n+1}|f_{n+1}|^2$ in the first equation and $p_{n-1}|p_{n-1}|^2$ in the second - terms absent in Eq. (B16) of model A. At last, the second transformation U_2 in Eq. (B14) rotates Eq. (B21) to (again only the equation of motion for the component α_n is given for the sake of space)

$$\begin{aligned} i\dot{\alpha}_n &= 4\alpha_n + \frac{U}{64} \{ 2\sqrt{3} [\alpha_{n+1}|\alpha_{n+1}|^2 - \alpha_{n-1}|\alpha_{n-1}|^2 \\ &\quad - \alpha_{n+1}^2 \beta_{n+1}^* - \alpha_{n-1}^2 \beta_{n-1}^* \\ &\quad + \beta_{n+1}^2 \alpha_{n+1}^* - \beta_{n-1}^2 \alpha_{n-1}^* \\ &\quad - \beta_{n+1}|\beta_{n+1}|^2 - \beta_{n-1}|\beta_{n-1}|^2 \\ &\quad - 2|\alpha_{n+1}|^2 \beta_{n+1} - 2|\alpha_{n-1}|^2 \beta_{n-1} \\ &\quad + 2\alpha_{n+1}|\beta_{n+1}|^2 - 2\alpha_{n-1}|\beta_{n-1}|^2 \\ &\quad + [\dots] \}, \end{aligned} \quad (\text{B22})$$

We have only kept the *fully nonlocal* terms in the above expression, where [...] indicates all the remaining terms from Eq. (B22) involving order three terms which involve α_n and/or β_n - as those in Eq. (B17).

5. Symplectic scheme

For the numerical time evolution of model A and model B, we used symplectic integration schemes. We detail

here for *e.g.* model B - Eq.(15). The Hamiltonian associated to the equations of motion of model B is

$$\mathcal{H} = \sum_{n=1}^N \left[\sqrt{3}(a_n^* a_{n+1} + a_{n+1}^* a_n) + a_n^* b_{n+1} - 3a_{n+1}^* b_n - \sqrt{3}(b_{n+1}^* b_n + b_n^* b_{n+1}) + b_{n+1}^* a_n - 3b_n^* a_{n+1} + \frac{U}{2}(|a_n|^4 + |b_n|^4) \right]. \quad (\text{B23})$$

Writing $a_n = \frac{q_a(n) + ip_a(n)}{\sqrt{2}}$ and $b_n = \frac{q_b(n) + ip_b(n)}{\sqrt{2}}$, we split the Hamiltonian as

$$\mathcal{H}_1 = \sum_{i=1}^N \left[\sqrt{3}\{p_a(n)p_a(n+1) + q_a(n)q_a(n+1)\} - \sqrt{3}\{p_b(n)p_b(n+1) + q_b(n)q_b(n+1)\} \right], \quad (\text{B24})$$

$$\mathcal{H}_2 = \sum_{i=1}^N \left[-3\{p_a(n+1)p_b(n) + q_a(n+1)q_b(n)\} + \{p_a(n)p_b(n+1) + q_a(n)q_b(n+1)\} \right], \quad (\text{B25})$$

$$\mathcal{H}_3 = \sum_{i=1}^N \left[\frac{U}{8}\{q_a^2(n) + p_a^2(n)\}^2 + \frac{U}{8}\{q_b^2(n) + p_b^2(n)\}^2 \right]. \quad (\text{B26})$$

We further split $\mathcal{H}_1 = \mathcal{H}_{1A} + \mathcal{H}_{1B}$:

$$\mathcal{H}_{1A} = \sum_{i=1}^N \left[\sqrt{3}\{p_a(n)p_a(n+1) - p_b(n)p_b(n+1)\} \right], \quad (\text{B27})$$

$$\mathcal{H}_{1B} = \sum_{i=1}^N \left[\sqrt{3}\{q_a(n)q_a(n+1) - q_b(n)q_b(n+1)\} \right], \quad (\text{B28})$$

and $\mathcal{H}_2 = \mathcal{H}_{2A} + \mathcal{H}_{2B}$

$$\mathcal{H}_{2A} = \sum_{i=1}^N \left[-3p_a(n+1)p_b(n) + p_a(n)p_b(n+1) \right], \quad (\text{B29})$$

$$\mathcal{H}_{2B} = \sum_{i=1}^N \left[-3q_a(n+1)q_b(n) + q_a(n)q_b(n+1) \right]. \quad (\text{B30})$$

The operators $e^{\Delta t L_{\mathcal{H}}}$ which propagate the set of initial conditions $(q_a(n), p_a(n), q_b(n), p_b(n))$ at the time t to the

final values $(q'_a(n), p'_a(n), q'_b(n), p'_b(n))$ at the time $t + \Delta t$ are

$$e^{\Delta t L_{\mathcal{H}_{1A}}} : \begin{cases} q'_a(n) = q_a(n) + \sqrt{3}[p_a(n+1) + p_a(n-1)]\Delta t \\ p'_a(n) = p_a(n) \\ q'_b(n) = q_b(n) - \sqrt{3}[p_b(n+1) + p_b(n-1)]\Delta t \\ p'_b(n) = p_b(n) \end{cases} \quad (\text{B31})$$

$$e^{\Delta t L_{\mathcal{H}_{1B}}} : \begin{cases} q'_a(n) = q_a(n) \\ p'_a(n) = p_a(n) - \sqrt{3}[q_a(n+1) + q_a(n-1)]\Delta t \\ q'_b(n) = q_b(n) \\ p'_b(n) = p_b(n) + \sqrt{3}[q_b(n+1) + q_b(n-1)]\Delta t \end{cases} \quad (\text{B32})$$

$$e^{\Delta t L_{\mathcal{H}_{2A}}} : \begin{cases} q'_a(n) = q_a(n) + [p_b(n+1) - 3p_b(n-1)]\Delta t \\ p'_a(n) = p_a(n) \\ q'_b(n) = q_b(n) + [-3p_a(n+1) + p_a(n-1)]\Delta t \\ p'_b(n) = p_b(n) \end{cases} \quad (\text{B33})$$

$$e^{\Delta t L_{\mathcal{H}_{2B}}} : \begin{cases} q'_a(n) = q_a(n) \\ p'_a(n) = p_a(n) - [q_b(n+1) - 3q_b(n-1)]\Delta t \\ q'_b(n) = q_b(n) \\ p'_b(n) = p_b(n) - [-3q_a(n+1) + q_a(n-1)]\Delta t \end{cases} \quad (\text{B34})$$

$$e^{\Delta t L_{\mathcal{H}_3}} : \begin{cases} q'_a(n) = q_a \cos(\alpha_a \Delta t) + p_a \sin(\alpha_a \Delta t) \\ p'_a(n) = p_a \cos(\alpha_a \Delta t) - q_a \sin(\alpha_a \Delta t) \\ q'_b(n) = q_b \cos(\alpha_b \Delta t) + p_b \sin(\alpha_b \Delta t) \\ p'_b(n) = p_b \cos(\alpha_b \Delta t) - q_b \sin(\alpha_b \Delta t) \end{cases} \quad (\text{B35})$$

where $\alpha_i(n) = \frac{p_i^2(n) + q_i^2(n)}{2}$, ($i = a, b$). We use second order splitting ABC scheme for the numerical integration [38].

The initial condition IC_1 used for the simulations presented in Fig. 3 is shown in Fig. 9. It has non-zero amplitudes only in two unit cells located in the center of the network - as shown in Fig. 9.

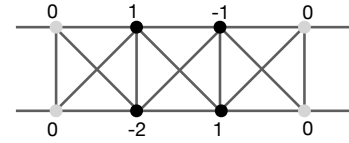


FIG. 9. (Color online) Spatial profile of the initial condition IC_1 used in Fig. 3.

The total norm of this initial condition is $S = \sum_{n=1}^N |a_n|^2 + |b_n|^2 = 7$. In Fig. 4 the curves are averaged over 48 initial conditions with random amplitudes concentrated in those same two unit cells of IC_1 in Fig. 9 generated so as to ensure the total norm $S = 7$.

Appendix C: Rotating the quantum interaction Hamiltonian \mathcal{H}_1^B

This rotations can be performed for the Bose-Hubbard Hamiltonian $\hat{\mathcal{H}}_B = \hat{\mathcal{H}}_0^B + \hat{\mathcal{H}}_1^B$ in Eqs. (17,18) for $\nu = 2$ expressed by the annihilation $\hat{c}_n = (\hat{a}_n, \hat{b}_n)$ and creation operators $\hat{c}_n^\dagger = (\hat{a}_n^\dagger, \hat{b}_n^\dagger)$ and parametrized by H_0, H_1 in Eqs. (A13,A14) under the condition $|w_1|^2 = |z_1|^2$

$$H_0 = \Gamma_0 \begin{pmatrix} 0 & -2z_1 w_1 \\ -2z_1^* w_1^* & 0 \end{pmatrix}, \quad (C1)$$

$$H_1 = \Gamma_1 \begin{pmatrix} z_1 w_1^* & z_1^2 \\ -(w_1^*)^2 & -z_1 w_1^* \end{pmatrix} \quad (C2)$$

with for $\Gamma_0 = |w_2|^2 - |z_2|^2$ and $\Gamma_1 = 2z_2 w_2$. The Hamiltonian $\hat{\mathcal{H}}_B = \hat{\mathcal{H}}_0^B + \hat{\mathcal{H}}_1^B$ reads

$$\hat{\mathcal{H}}_0^B = \sum_{n \in \mathbb{Z}} \left[-\frac{1}{2} (\hat{c}_n^{\dagger T} H_0 \hat{c}_n) - (\hat{c}_n^{\dagger T} H_1 \hat{c}_{n+1}) - \text{h.c.} \right], \quad (C3)$$

$$\hat{\mathcal{H}}_1^B = \frac{U}{2} \sum_{n \in \mathbb{Z}} \left[\hat{a}_n^\dagger \hat{a}_n^\dagger \hat{a}_n \hat{a}_n + \hat{b}_n^\dagger \hat{b}_n^\dagger \hat{b}_n \hat{b}_n \right]. \quad (C4)$$

We partially detangle the Hamiltonians $\hat{\mathcal{H}}_0^B$ and $\hat{\mathcal{H}}_1^B$ separately, applying first the unitary transformation U_1 in Eq. (A7) assuming $|w_1|^2 = |z_1|^2$, and then the unit cell redefinition T in Eq. (A8). We start with $\hat{\mathcal{H}}_0^B$.

The unitary transformation U_1

$$U_1 = e^{i\theta_1} \begin{pmatrix} z_1 & w_1 \\ -w_1^* & z_1^* \end{pmatrix} \quad (C5)$$

maps the operators $\hat{\psi}_n^\dagger = (\hat{a}_n^\dagger, \hat{b}_n^\dagger)$ and $\hat{\psi}_n = (\hat{a}_n, \hat{b}_n)$ to the creation $\hat{\xi}_n^\dagger = (\hat{p}_n^\dagger, \hat{f}_n^\dagger)$ and annihilation operators $\hat{\xi}_n = (\hat{p}_n, \hat{f}_n)$. The Hamiltonian $\hat{\mathcal{H}}_0^B$ in Eq. (C3) turns

$$\hat{\mathcal{H}}_0^B = \sum_n \left[-\frac{1}{2} (\hat{\xi}_n^{\dagger T} H_0^{(3)} \hat{\xi}_n) - (\hat{\xi}_n^{\dagger T} H_1^{(3)} \hat{\xi}_{n+1}) - \text{h.c.} \right] \quad (C6)$$

with $H_0^{(3)}$ and $H_1^{(3)}$ in Eqs. (A11,A12) - here recalled

$$H_0^{(3)} = \begin{pmatrix} |w_2|^2 - |z_2|^2 & 0 \\ 0 & |z_2|^2 - |w_2|^2 \end{pmatrix}, \quad (C7)$$

$$H_1^{(3)} = \begin{pmatrix} 0 & 2z_2 w_2 \\ 0 & 0 \end{pmatrix}. \quad (C8)$$

The unit cell redefinition T in Eq. (A8) - here recalled

$$\begin{cases} \hat{p}_n & \mapsto \hat{p}_n \\ \hat{f}_n & \mapsto \hat{f}_{n-1} \end{cases} \quad (C9)$$

redefine the Hamiltonian $\hat{\mathcal{H}}_0^B$ in Eq. (C6) turns to

$$\hat{\mathcal{H}}_0^B = \sum_n \left\{ (|z_2|^2 - |w_2|^2) (-\hat{p}_n^\dagger \hat{p}_n + \hat{f}_n^\dagger \hat{f}_n) + 2w_2 z_2 \hat{p}_n^\dagger \hat{f}_n + 2w_2^* z_2^* \hat{p}_n \hat{f}_n^\dagger \right\}. \quad (C10)$$

For the interaction Hamiltonian $\hat{\mathcal{H}}_1^B$ in Eq. (C4), let us state explicitly the unitary transformation U_1 in Eq. (C5) applied to the operators $\hat{a}_n^\dagger, \hat{b}_n^\dagger, \hat{a}_n, \hat{b}_n$ and $\hat{p}_n^\dagger, \hat{f}_n^\dagger, \hat{p}_n, \hat{f}_n$, namely

$$\begin{cases} \hat{a}_n = e^{i\theta_1} (z_1 \hat{p}_n + w_1 \hat{f}_n) \\ \hat{b}_n = e^{i\theta_1} (-w_1^* \hat{p}_n + z_1^* \hat{f}_n) \\ \hat{a}_n^\dagger = e^{-i\theta_1} (z_1^* \hat{p}_n^\dagger + w_1^* \hat{f}_n^\dagger) \\ \hat{b}_n^\dagger = e^{-i\theta_1} (-w_1 \hat{p}_n^\dagger + z_1 \hat{f}_n^\dagger) \end{cases} \quad (C11)$$

Let us recall the commutativity between creation and annihilation operators, as well as of operator over different coordinates (*e.g.* $\hat{p}_n^\dagger \hat{f}_n^\dagger = \hat{f}_n^\dagger \hat{p}_n^\dagger$). The first interaction term $\hat{a}_n^\dagger \hat{a}_n^\dagger \hat{a}_n \hat{a}_n$ turns

$$\begin{aligned} \hat{a}_n^\dagger \hat{a}_n^\dagger \hat{a}_n \hat{a}_n &= \\ &= (z_1^* \hat{p}_n^\dagger + w_1^* \hat{f}_n^\dagger) (z_1^* \hat{p}_n^\dagger + w_1^* \hat{f}_n^\dagger) \\ &\quad \times (z_1 \hat{p}_n + w_1 \hat{f}_n) (z_1 \hat{p}_n + w_1 \hat{f}_n) \\ &= (z_1^{*2} \hat{p}_n^\dagger \hat{p}_n^\dagger + 2z_1^* w_1^* \hat{p}_n^\dagger \hat{f}_n^\dagger + w_1^{*2} \hat{f}_n^\dagger \hat{f}_n^\dagger) \\ &\quad \times (z_1^2 \hat{p}_n \hat{p}_n + 2z_1 w_1 \hat{p}_n \hat{f}_n + w_1^2 \hat{f}_n \hat{f}_n) \\ &= |z_1|^4 \hat{p}_n^\dagger \hat{p}_n^\dagger \hat{p}_n \hat{p}_n + 2z_1^* |z_1|^2 w_1 \hat{p}_n^\dagger \hat{p}_n^\dagger \hat{p}_n \hat{f}_n \\ &\quad + z_1^{*2} w_1^2 \hat{p}_n^\dagger \hat{p}_n^\dagger \hat{f}_n \hat{f}_n + 2z_1 |z_1|^2 w_1^* \hat{p}_n^\dagger \hat{f}_n^\dagger \hat{p}_n \hat{p}_n \\ &\quad + 4|z_1|^2 |w_1|^2 \hat{p}_n^\dagger \hat{f}_n^\dagger \hat{p}_n \hat{f}_n + 2z_1^* w_1 |w_1|^2 \hat{p}_n^\dagger \hat{f}_n^\dagger \hat{f}_n \hat{f}_n \\ &\quad + z_1^2 w_1^{*2} \hat{f}_n^\dagger \hat{f}_n^\dagger \hat{p}_n \hat{p}_n + 2z_1 w_1^* |w_1|^2 \hat{f}_n^\dagger \hat{f}_n^\dagger \hat{p}_n \hat{f}_n \\ &\quad + |w_1|^4 \hat{f}_n^\dagger \hat{f}_n^\dagger \hat{f}_n \hat{f}_n \end{aligned} \quad (C12)$$

The second interaction term $\hat{b}_n^\dagger \hat{b}_n^\dagger \hat{b}_n \hat{b}_n$ turns

$$\begin{aligned} \hat{b}_n^\dagger \hat{b}_n^\dagger \hat{b}_n \hat{b}_n &= \\ &= (-w_1 \hat{p}_n^\dagger + z_1 \hat{f}_n^\dagger) (-w_1 \hat{p}_n^\dagger + z_1 \hat{f}_n^\dagger) \\ &\quad \times (-w_1^* \hat{p}_n + z_1^* \hat{f}_n) (-w_1^* \hat{p}_n + z_1^* \hat{f}_n) \\ &= (w_1^2 \hat{p}_n^\dagger \hat{p}_n^\dagger - 2w_1 z_1 \hat{p}_n^\dagger \hat{f}_n^\dagger + z_1^2 \hat{f}_n^\dagger \hat{f}_n^\dagger) \\ &\quad \times (w_1^{*2} \hat{p}_n \hat{p}_n - 2w_1^* z_1^* \hat{p}_n \hat{f}_n + z_1^{*2} \hat{f}_n \hat{f}_n) \\ &= |w_1|^4 \hat{p}_n^\dagger \hat{p}_n^\dagger \hat{p}_n \hat{p}_n - 2z_1^* |w_1|^2 w_1 \hat{p}_n^\dagger \hat{p}_n^\dagger \hat{p}_n \hat{f}_n \\ &\quad + z_1^{*2} w_1^2 \hat{p}_n^\dagger \hat{p}_n^\dagger \hat{f}_n \hat{f}_n - 2z_1 |w_1|^2 w_1^* \hat{p}_n^\dagger \hat{f}_n^\dagger \hat{p}_n \hat{p}_n \\ &\quad + 4|z_1|^2 |w_1|^2 \hat{p}_n^\dagger \hat{f}_n^\dagger \hat{p}_n \hat{f}_n - 2z_1^* |z_1|^2 w_1 \hat{p}_n^\dagger \hat{f}_n^\dagger \hat{f}_n \hat{f}_n \\ &\quad + z_1^2 w_1^{*2} \hat{f}_n^\dagger \hat{f}_n^\dagger \hat{p}_n \hat{p}_n - 2z_1 |z_1|^2 w_1^* \hat{f}_n^\dagger \hat{f}_n^\dagger \hat{p}_n \hat{f}_n \\ &\quad + |z_1|^4 \hat{f}_n^\dagger \hat{f}_n^\dagger \hat{f}_n \hat{f}_n \end{aligned} \quad (C13)$$

The sum of these terms yields

$$\begin{aligned}
& \hat{a}_n^\dagger \hat{a}_n^\dagger \hat{a}_n \hat{a}_n + \hat{b}_n^\dagger \hat{b}_n^\dagger \hat{b}_n \hat{b}_n = \\
& = (|z_1|^4 + |w_1|^4) \hat{p}_n^\dagger \hat{p}_n^\dagger \hat{p}_n \hat{p}_n \\
& + 2z_1^* w_1 (|z_1|^2 - |w_1|^2) \hat{p}_n^\dagger \hat{p}_n^\dagger \hat{p}_n \hat{f}_n \\
& + 2z_1^{*2} w_1^2 \hat{p}_n^\dagger \hat{p}_n^\dagger \hat{f}_n \hat{f}_n \\
& + 2z_1 w_1^* (|z_1|^2 - |w_1|^2) \hat{p}_n^\dagger \hat{f}_n^\dagger \hat{p}_n \hat{p}_n \\
& + 8|z_1|^2 |w_1|^2 \hat{p}_n^\dagger \hat{f}_n^\dagger \hat{p}_n \hat{f}_n \\
& + 2z_1^* w_1 (|w_1|^2 - |z_1|^2) \hat{p}_n^\dagger \hat{f}_n^\dagger \hat{f}_n \hat{f}_n \\
& + 2z_1^2 w_1^{*2} \hat{f}_n^\dagger \hat{f}_n^\dagger \hat{p}_n \hat{p}_n \\
& + 2z_1 w_1^* (|w_1|^2 - |z_1|^2) \hat{f}_n^\dagger \hat{f}_n^\dagger \hat{p}_n \hat{f}_n \\
& + (|z_1|^4 + |w_1|^4) \hat{f}_n^\dagger \hat{f}_n^\dagger \hat{f}_n \hat{f}_n
\end{aligned} \tag{C14}$$

The assumption $|w_1|^2 = |z_1|^2$ simplifies Eq. (C14) to

$$\begin{aligned}
& \hat{a}_n^\dagger \hat{a}_n^\dagger \hat{a}_n \hat{a}_n + \hat{b}_n^\dagger \hat{b}_n^\dagger \hat{b}_n \hat{b}_n = \\
& = 2|z_1|^4 \hat{p}_n^\dagger \hat{p}_n^\dagger \hat{p}_n \hat{p}_n + 2z_1^{*2} w_1^2 \hat{p}_n^\dagger \hat{p}_n^\dagger \hat{f}_n \hat{f}_n \\
& + 8|z_1|^4 \hat{p}_n^\dagger \hat{f}_n^\dagger \hat{p}_n \hat{f}_n + 2z_1^2 w_1^{*2} \hat{f}_n^\dagger \hat{f}_n^\dagger \hat{p}_n \hat{p}_n \\
& + 2|z_1|^4 \hat{f}_n^\dagger \hat{f}_n^\dagger \hat{f}_n \hat{f}_n
\end{aligned} \tag{C15}$$

The unit cell redefinition in Eq. (C9) turns the R.H.S of Eq. (C15) to

$$\begin{aligned}
& \hat{a}_n^\dagger \hat{a}_n^\dagger \hat{a}_n \hat{a}_n + \hat{b}_n^\dagger \hat{b}_n^\dagger \hat{b}_n \hat{b}_n = \\
& = 2|z_1|^4 \hat{p}_n^\dagger \hat{p}_n^\dagger \hat{p}_n \hat{p}_n + 2z_1^{*2} w_1^2 \hat{p}_n^\dagger \hat{p}_n^\dagger \hat{f}_{n+1} \hat{f}_{n+1} \\
& + 8|z_1|^4 \hat{p}_n^\dagger \hat{f}_{n+1}^\dagger \hat{p}_n \hat{f}_{n+1} + 2z_1^2 w_1^{*2} \hat{f}_{n+1}^\dagger \hat{f}_{n+1}^\dagger \hat{p}_n \hat{p}_n \\
& + 2|z_1|^4 \hat{f}_{n+1}^\dagger \hat{f}_{n+1}^\dagger \hat{f}_{n+1} \hat{f}_{n+1}
\end{aligned} \tag{C16}$$

and ultimately to the rotated Hamiltonian $\hat{\mathcal{H}}_1^B$

$$\begin{aligned}
\hat{\mathcal{H}}_1^B = U \sum_n \Big\{ & |z_1|^4 \left[\hat{p}_n^\dagger \hat{p}_n^\dagger \hat{p}_n \hat{p}_n + \hat{f}_n^\dagger \hat{f}_n^\dagger \hat{f}_n \hat{f}_n + 4\hat{p}_n^\dagger \hat{f}_{n+1}^\dagger \hat{p}_n \hat{f}_{n+1} \right] \\
& + z_1^{*2} w_1^2 \hat{p}_n^\dagger \hat{p}_n^\dagger \hat{f}_{n+1} \hat{f}_{n+1} + z_1^* w_1^{*2} \hat{p}_n \hat{p}_n \hat{f}_{n+1}^\dagger \hat{f}_{n+1}^\dagger \Big\}
\end{aligned} \tag{C17}$$

Notably, the rotated Hamiltonians $\hat{\mathcal{H}}_0^B$ in Eq. (C10) and $\hat{\mathcal{H}}_1^B$ in Eq. (C17) expressed in terms of annihilation and creation operators $\hat{p}_n^\dagger, \hat{f}_n^\dagger$ and \hat{p}_n, \hat{f}_n are the same as those in $\hat{\mathcal{H}}_0^G$ in Eq. (B10) and $\hat{\mathcal{H}}_1^G$ in Eq. (B11) after the substitution $\hat{p}_n \rightarrow \hat{h}_n, \hat{f}_n \rightarrow \hat{f}_n, \hat{p}_n^\dagger \rightarrow \hat{h}_n^*, \hat{f}_n^\dagger \rightarrow \hat{f}_n^*$.

Appendix D: Two Interacting Particles

1. Two Interacting particles - Fock space representation

We represent two interacting distinguishable particles in the two-bands lattice Eqs. (17,18) with the following

basis for $1 \leq n, k \leq N$ with periodic boundary conditions

$$\begin{aligned}
|n, k\rangle_a &= \hat{a}_n^\dagger \hat{a}_k^\dagger |0\rangle & |n, k\rangle_b &= \hat{b}_n^\dagger \hat{b}_k^\dagger |0\rangle \\
|n, k\rangle_{a,b} &= \hat{a}_n^\dagger \hat{b}_k^\dagger |0\rangle & |n, k\rangle_{b,a} &= \hat{b}_k^\dagger \hat{a}_n^\dagger |0\rangle
\end{aligned} \tag{D1}$$

The 2IP wave-function $|\psi\rangle$

$$\begin{aligned}
|\psi\rangle &= \sum_{n,k=1}^N X_{n,k} |n, k\rangle_a + Z_{n,k} |n, k\rangle_b \\
&+ \sum_{n,k=1}^N Y_{n,k} |n, k\rangle_{a,b} + W_{n,k} |n, k\rangle_{b,a}
\end{aligned} \tag{D2}$$

evolve according to a two dimensional Schrödinger system of equations

$$\begin{aligned}
i\dot{\varphi}_{n,k} &= [A + UV] \varphi_{n,k} + T_n \varphi_{n+1,k} + T_n^\dagger \varphi_{n-1,k} \\
&+ T_k \varphi_{n,k+1} + T_k^\dagger \varphi_{n,k-1}
\end{aligned} \tag{D3}$$

with $\varphi_{n,k} = (X_{n,k}, Y_{n,k}, W_{n,k}, Z_{n,k})^T$.

The matrices A, V, T_n, T_k which define Eq. (D3) are obtained via the following generic and standard procedure (here stated for any $\nu = 2$ network):

1. consider the motion equation

$$i \frac{\partial}{\partial t} |\psi\rangle = \hat{\mathcal{H}}_B |\psi\rangle \tag{D4}$$

associated to the $\nu = 2$ Bose-Hubbard Hamiltonian $\hat{\mathcal{H}}_B = \hat{\mathcal{H}}_0^B + \hat{\mathcal{H}}_1^B$ in Eqs. (17,18)

2. substitute the expansion of the wave function $|\psi\rangle$ Eq. (D2) in the motion equation (D4).
3. unfold the products on the r.h.s of Eq.(D4) and shift the indexes of the basis vectors. This recast the motion equation to

$$\begin{aligned}
& i \sum_{n,k=1}^N \dot{X}_{n,k} |n, k\rangle_a + \dot{Z}_{n,k} |n, k\rangle_b \\
& + i \sum_{n,k=1}^N \dot{Y}_{n,k} |n, k\rangle_{a,b} + \dot{W}_{n,k} |n, k\rangle_{b,a} = \\
& \sum_{n,k=1}^N \left\{ p_1 |n, k\rangle_a + p_2 |n, k\rangle_b + p_3 |n, k\rangle_{a,b} + p_4 |n, k\rangle_{b,a} \right\}
\end{aligned} \tag{D5}$$

with p_1, \dots, p_4 are homogeneous linear polynomial in $\varphi_{n,k} = (X_{n,k}, Y_{n,k}, W_{n,k}, Z_{n,k})^T$

4. Eq. D5 then yields Eq. D3 by separating the onsite terms in the matrix A , the hopping terms along $\{n, n \pm 1\}$ in the matrix T_n, T_n^\dagger , as well as the hopping terms along $\{k, k \pm 1\}$ in the matrix T_k, T_k^\dagger .

In the case of Bose-Hubbard Hamiltonian $\hat{\mathcal{H}}_B = \hat{\mathcal{H}}_0^B + \hat{\mathcal{H}}_1^B$ in Eqs. (17,18) with matrices H_0, H_1 parameterized in Eqs. (5,6), the onsite matrices A is

$$A = 2\Gamma_0 \begin{pmatrix} |z_1|^2 - |w_1|^2 & -z_1 w_1 & -z_1 w_1 & 0 \\ -z_1^* w_1^* & 0 & 0 & -z_1 w_1 \\ -z_1^* w_1^* & 0 & 0 & -z_1 w_1 \\ 0 & -z_1^* w_1^* & -z_1^* w_1^* & |w_1|^2 - |z_1|^2 \end{pmatrix} \quad (\text{D6})$$

while the hopping matrices T_n, T_k are

$$T_n = \Gamma_1 \begin{pmatrix} z_1 w_1^* & 0 & z_1^2 & 0 \\ 0 & z_1 w_1^* & 0 & z_1^2 \\ -(w_1^*)^2 & 0 & -z_1 w_1^* & 0 \\ 0 & -(w_1^*)^2 & 0 & -z_1 w_1^* \end{pmatrix}, \quad (\text{D7})$$

$$T_k = \Gamma_1 \begin{pmatrix} z_1 w_1^* & z_1^2 & 0 & 0 \\ -(w_1^*)^2 & -z_1 w_1^* & 0 & 0 \\ 0 & 0 & z_1 w_1^* & z_1^2 \\ 0 & 0 & -(w_1^*)^2 & -z_1 w_1^* \end{pmatrix} \quad (\text{D8})$$

for $\Gamma_0 = |w_2|^2 - |z_2|^2$ and $\Gamma_1 = 2z_2 w_2$. The BH interaction $\hat{\mathcal{H}}_1^B$ applies only when both particles are on the same site - hence, the Kronecker delta $\delta_{n,k}$. The matrix V reads

$$V = \begin{pmatrix} \delta_{n,k} & 0 & 0 & 0 \\ 0 & 0 & 0 & 0 \\ 0 & 0 & 0 & 0 \\ 0 & 0 & 0 & \delta_{n,k} \end{pmatrix}. \quad (\text{D9})$$

The numerical simulations of the time evolution of Eq. (D3) of two-interacting particles for both Model A and model B have been performed using the commercial software Mathematica employing the fourth-order explicit Runge-Kutta scheme.

-
- [1] P. W. Anderson, “Absence of diffusion in certain random lattices,” *Phys. Rev.* **109**, 1492–1505 (1958).
- [2] D.M. Basko, I.L. Aleiner, and B.L. Altshuler, “Metal-insulator transition in a weakly interacting many-electron system with localized single-particle states,” *Ann. Phys.* **321**, 1126 – 1205 (2006).
- [3] I. L. Aleiner, B. L. Altshuler, and G. V. Shlyapnikov, “A finite-temperature phase transition for disordered weakly interacting bosons in one dimension,” *Nat. Phys.* **6**, 900–904 (2010).
- [4] Dmitry A. Abanin, Ehud Altman, Immanuel Bloch, and Maksym Serbyn, “Colloquium: Many-body localization, thermalization, and entanglement,” *Rev. Mod. Phys.* **91**, 021001 (2019).
- [5] T V Lapyteva, M V Ivanchenko, and S Flach, “Nonlinear lattice waves in heterogeneous media,” *J Phys. A: Math. Theor.* **47**, 493001 (2014).
- [6] Ihor Vakulchyk, Mikhail V. Fistul, and Sergej Flach, “Wave packet spreading with disordered nonlinear discrete-time quantum walks,” *Phys. Rev. Lett.* **122**, 040501 (2019).
- [7] Daniel Leykam, Alexei Andreanov, and Sergej Flach, “Artificial flat band systems: from lattice models to experiments,” *Adv. Phys.: X* **3**, 1473052 (2018).
- [8] Daniel Leykam and Sergej Flach, “Perspective: Photonic flatbands,” *APL Phot.* **3**, 070901 (2018).
- [9] Sergej Flach, Daniel Leykam, Joshua D. Bodyfelt, Peter Matthies, and Anton S. Desyatnikov, “Detangling flat bands into Fano lattices,” *EPL (Europhysics Letters)* **105**, 30001 (2014).
- [10] Wulayimu Maimaiti, Alexei Andreanov, Hee Chul Park, Oleg Gendelman, and Sergej Flach, “Compact localized states and flat-band generators in one dimension,” *Phys. Rev. B* **95**, 115135 (2017).
- [11] M. Röntgen, C. V. Morfonios, and P. Schmelcher, “Compact localized states and flat bands from local symmetry partitioning,” *Phys. Rev. B* **97**, 035161 (2018).
- [12] L A Toikka and A Andreanov, “Necessary and sufficient conditions for flat bands in m-dimensional n-band lattices with complex-valued nearest-neighbour hopping,” *J Phys. A: Math. Theor* **52**, 02LT04 (2018).
- [13] Wulayimu Maimaiti, Sergej Flach, and Alexei Andreanov, “Universal $d = 1$ flat band generator from compact localized states,” *Phys. Rev. B* **99**, 125129 (2019).
- [14] Daniel Leykam, Sergej Flach, Omri Bahat-Treidel, and Anton S. Desyatnikov, “Flat band states: Disorder and nonlinearity,” *Phys. Rev. B* **88**, 224203 (2013).
- [15] Joshua D. Bodyfelt, Daniel Leykam, Carlo Danieli, Xiaoquan Yu, and Sergej Flach, “Flatbands under correlated perturbations,” *Phys. Rev. Lett.* **113**, 236403 (2014).
- [16] Carlo Danieli, Joshua D. Bodyfelt, and Sergej Flach, “Flat-band engineering of mobility edges,” *Phys. Rev. B* **91**, 235134 (2015).
- [17] Daniel Leykam, Joshua D. Bodyfelt, Anton S. Desyatnikov, and Sergej Flach, “Localization of weakly disordered flat band states,” *Eur. Phys. J. B* **90**, 1 (2017).
- [18] Daniel Leykam, Sergej Flach, and Y. D. Chong, “Flat bands in lattices with non-hermitian coupling,” *Phys. Rev. B* **96**, 064305 (2017).
- [19] C. Danieli and T. Mithun, “Casting dissipative compact states in coherent perfect absorbers,” *Phys. Rev. Research* **2**, 013054 (2020).
- [20] Magnus Johansson, Uta Naether, and Rodrigo A. Vencio, “Compactification tuning for nonlinear localized modes in sawtooth lattices,” *Phys. Rev. E* **92**, 032912 (2015).
- [21] G. Gligorić, A. Maluckov, Lj. Hadžievski, Sergej Flach, and Boris A. Malomed, “Nonlinear localized flat-band modes with spin-orbit coupling,” *Phys. Rev. B* **94**, 144302 (2016).

- [22] Ajith Ramachandran, Carlo Danieli, and Sergej Flach, “Fano resonances in flat band networks,” in *Fano Resonances in Optics and Microwaves: Physics and Applications*, edited by Eugene Kamenetskii, Almas Sadreev, and Andrey Miroshnichenko (Springer International Publishing, Cham, 2018) pp. 311–329.
- [23] C. Danieli, A. Maluckov, and S. Flach, “Compact discrete breathers on flat-band networks,” *Low Temp. Phys.* **44**, 678–687 (2018).
- [24] Naoyuki Masumoto, Na Young Kim, Tim Byrnes, Kenichiro Kusudo, Andreas Löffler, Sven Höfling, Alfred Forchel, and Yoshihisa Yamamoto, “Exciton–polariton condensates with flat bands in a two-dimensional kagome lattice,” *New J. Phys.* **14**, 065002 (2012).
- [25] Seababrata Mukherjee, Alexander Spracklen, Debaditya Choudhury, Nathan Goldman, Patrik Öhberg, Erika Andersson, and Robert R. Thomson, “Observation of a localized flat-band state in a photonic Lieb lattice,” *Phys. Rev. Lett.* **114**, 245504 (2015).
- [26] Rodrigo A. Vicencio, Camilo Cantillano, Luis Morales-Inostroza, Bastián Real, Cristian Mejía-Cortés, Steffen Weimann, Alexander Szameit, and Mario I. Molina, “Observation of localized states in Lieb photonic lattices,” *Phys. Rev. Lett.* **114**, 245503 (2015).
- [27] Shintaro Taie, Hideki Ozawa, Tomohiro Ichinose, Takuei Nishio, Shuta Nakajima, and Yoshiro Takahashi, “Coherent driving and freezing of bosonic matter wave in an optical Lieb lattice,” *Sci. Adv.* **1** (2015), 10.1126/sciadv.1500854.
- [28] Steffen Weimann, Luis Morales-Inostroza, Bastián Real, Camilo Cantillano, Alexander Szameit, and Rodrigo A. Vicencio, “Transport in sawtooth photonic lattices,” *Opt. Lett.* **41**, 2414–2417 (2016).
- [29] Shiqiang Xia, Carlo Danieli, Wenchao Yan, Denghui Li, Shiqi Xia, Jina Ma, Hai Lu, Daohong Song, Liqin Tang, Sergej Flach, and Zhigang Chen, “Observation of quincunx-shaped and dipole-like flatband states in photonic rhombic lattices without band-touching,” *APL Phot.* **5**, 016107 (2020).
- [30] Seababrata Mukherjee, Marco Di Liberto, Patrik Öhberg, Robert R. Thomson, and Nathan Goldman, “Experimental observation of Aharonov-Bohm cages in photonic lattices,” *Phys. Rev. Lett.* **121**, 075502 (2018).
- [31] Goran Gligorić, Petra P. Beličev, Daniel Leykam, and Aleksandra Maluckov, “Nonlinear symmetry breaking of Aharonov-Bohm cages,” *Phys. Rev. A* **99**, 013826 (2019).
- [32] Marco Di Liberto, Seababrata Mukherjee, and Nathan Goldman, “Nonlinear dynamics of aharonov-bohm cages,” *Phys. Rev. A* **100**, 043829 (2019).
- [33] Julien Vidal, Benoît Douçot, Rémy Mosseri, and Patrick Butaud, “Interaction induced delocalization for two particles in a periodic potential,” *Phys. Rev. Lett.* **85**, 3906–3909 (2000).
- [34] Carlo Danieli, Mithun Thudiyangal, Alexei Andreanov, and Sergej Flach, “Caging of short-range interactions in all bands flat lattices: Part II,” (2020), [arXiv:2004.11880 \[cond-mat.quant-gas\]](https://arxiv.org/abs/2004.11880).
- [35] Murad Tovmasyan, Sebastiano Peotta, Long Liang, Päivi Törmä, and Sebastian D. Huber, “Preformed pairs in flat bloch bands,” *Phys. Rev. B* **98**, 134513 (2018).
- [36] Simon Tilleke, Mirko Daumann, and Thomas Dahm, “Nearest neighbour particle-particle interaction in fermionic quasi one-dimensional flat band lattices,” *Zeitschrift für Naturforschung A*, 20190371 (2020).
- [37] Carlo Danieli, Alexei Andreanov, and Sergej Flach, “Many-body flatband localization,” (2020), [arXiv:2004.11928 \[cond-mat.stat-mech\]](https://arxiv.org/abs/2004.11928).
- [38] C. Danieli, B. Many Manda, T. Mithun, and Ch. Skokos, “Computational efficiency of numerical integration methods for the tangent dynamics of many-body hamiltonian systems in one and two spatial dimensions,” *Mathematics in Engineering* **1**, 447 (2019).